Marine Geology 481 (2025) 107477

Contents lists available at ScienceDirect

Marine Geology

journal homepage: www.elsevier.com/locate/margo

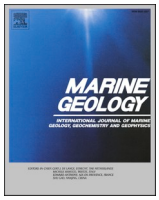

Research Article

Rapid, complex back barrier pedestal formation preconditions washover deposition on the southeast Indian coast

Chris Gouramanis [a,*], Seshachalam Srinivasalu [b], Andasabari Karthik [c], Dat T. Pham [d], Stephen Carson [e], Adam D. Switzer [f,g]

[a] Research School of Earth Sciences, The Australian National University, Canberra 2601, Australia
[b] Institute of Ocean Management, Anna University, Chennai 600025, India
[c] National Institute of Ocean Technology, Ministry of Earth Sciences, Chennai 600100, India
[d] VNU University of Science, Vietnam National University, Ha Noi, Viet Nam
[e] Mabbett, Mabbett House, 10 Sandyford Place, Glasgow G3 7NB, UK
[f] Earth Observatory of Singapore, Nanyang Technological University, 639798, Singapore
[g] The Asian School of the Environment, Nanyang Technological University, 639798, Singapore

ARTICLE INFO

Editor: Shu Gao

Keywords:
Ground Penetrating Radar (GPR)
Cyclone
Sedimentology
Stratigraphy
India
Onlapping beds
Terminal foresets

ABSTRACT

Washover deposits formed by overwash are important deposits for evaluating the stratigraphy and evolution of coastal environments. Examination of preserved washover fans can provide a palaeotempestological record that inform past and recent coastal risk with a view to predicting future coastal risk. The recognition of past washover deposits in coastal systems requires detailed knowledge of the internal structure of recent deposits including washover fans. We used very high frequency Ground Penetrating Radar and satellite imagery to examine the internal architecture of the 31st December 2011 Cyclone Thane surge-generated washover deposit on the beach that blocked the Thenpennai River at Thazhamkuda, near Cuddalore in Tamil Nadu Province, southeastern India. Cyclone Thane overwash overtopped the beach and deposited sediments on the contemporary beach and behind the beach within the former channel of the blocked river. The modern washover fan thus contains sediments that are preserved subaqueously and subaerially. We demonstrate that the internal architecture of the fan at Thazhamkuda is largely controlled by the pre-existing topography, and erosional and depositional processes as the cyclone washed sediment inland. At the landward margin of the fan, terminal foreset bedding is preserved and is likely to be one of the only features that can discriminate storm over tsunami deposits.

1. Introduction

Analysis of modern storm surge sedimentary deposits has largely focused on the sedimentology, sedimentary structures, and stratigraphy of washover fans (e.g. Morton, 1979; Schwartz, 1975; Schwartz, 1982; Soria et al., 2017) or on sheet flooded deposits (e.g. Soria et al., 2016). The architecture and formation of washover fans has been examined by numerous authors, predominantly in the southeastern United States of America (e.g. Hayes, 1967; Morton, 1978; Morton, 1979; Schwartz, 1975; Schwartz, 1982; Leatherman and Williams, 1977; Leatherman et al., 1977; Rodriguez et al., 2020), but also in Asia (e.g. Brill et al., 2016; Ganzei et al., 2010; Pham et al., 2017; Phantuwongraj et al., 2013; Soria et al., 2017; Soria et al., 2021; Yap et al., 2021), Australia (e.g. May et al., 2017; Switzer and Jones, 2008), Pacific Islands (e.g. Hong et al., 2018; Kosciuch et al., 2018), Indian Ocean (e.g. Haque et al., 2021; Gouramanis et al., 2024) and Africa (e.g. Dixon et al., 2015; Benamri et al., 2023).

Much of the early scholarly work focused on the identification and development of storm deposits in different coastal environments, such as a barrier islands, spits or coastal terraces (e.g. Hayes, 1967; Leatherman and Williams, 1977; Leatherman et al., 1977; Morton, 1978; Morton, 1979; Morton and Sallenger, 2003; Schwartz, 1975; Schwartz, 1982). These environments are commonly backed by a stationary body of water, e.g. lagoon, lake, blocked river or estuary, that the storm deposited sediments can flow into (e.g. Liu and Fearn, 2000) or that impede the development of storm surge fans (e.g. Morton, 1978; Morton, 1979; Morton and Sallenger, 2003; Schwartz, 1975; Schwartz, 1982; Sedgwick and Davis, 2003). Where these storm deposits are

* Corresponding author.
E-mail address: chris.gouramanis@anu.edu.au (C. Gouramanis).

https://doi.org/10.1016/j.margeo.2025.107477
Received 9 September 2024; Received in revised form 9 January 2025; Accepted 11 January 2025
Available online 16 January 2025

preserved in the sediment and geological record, they serve as indicators of past overwash. Examination of the geological records of storms provides a detailed storm history to contribute to future risk adaptation and mitigation strategies (e.g. Donnelly et al., 2001; Donnelly and Woodruff, 2007; Liu and Fearn, 1993). Two primary challenges exist to achieve these outcomes. The first challenge remains to identify the deposits from an event from the background sedimentary environment, which is difficult when the deposited sediment is similar to the depositional environment sediment (e.g. Wang and Horwitz, 2006, Gouramanis et al., 2024, c.f. Liu and Fearn, 1993). The second challenge remains to correctly attribute a deposit to an event, as tsunami and meteotsunami (e.g. Pattiaratchi and Wijeratne, 2015) are also known to inundate coastal environments (Kortekaas and Dawson, 2007; Morton et al., 2007; Pham et al., 2017; Phantuwongraj and Choowong, 2011; Yap et al., 2021; Gouramanis et al., 2017).

One of the few diagnostic characteristics for distinguishing between the causes of coastal washover deposits are steeply dipping (up to 30°) foreset beds commonly found at the landward margin of a storm fan (e.g. Morton, 1978; Morton, 1979; Phantuwongraj and Choowong, 2011; Schwartz, 1975; Schwartz, 1982; Soria et al., 2021). Terminal foresets occur where storm surge encounters stationary water causing a sudden decrease in flow velocity resulting in the deposition of sediments at the terminus of the fan (Schwartz, 1975; Schwartz, 1982).

Ground Penetrating Radar (GPR) offers a data-rich, non-destructive method for exploring the stratigraphy and evolution of coastal washover deposits (e.g. Bristow, 2013; Jol and Bristow, 2003; Switzer et al., 2020; Neal, 2004). The use of GPR to investigate storm history has focused largely on examination of the erosive signatures when beach face and dune sediments are scoured during high-intensity storm events and subsequent recovery during inter-storm periods (e.g. Buynevich et al., 2007; Lindhorst et al., 2008). Less research has utilised GPR to explore the depositional nature of storm deposits (e.g. Lindhorst et al., 2008; May et al., 2017; Soria et al., 2021; Wang and Horwitz, 2006).

In this study we examine the sediment dynamics that occur when the Thenpennai River mouth recloses after a breach and the subsequent evolution of the barrier following the landfall of Cyclone Thane on the coastline of Tamil Nadu, southeast India in 2011. We use GPR to examine the stratigraphy and evolution of a large fan formed by Cyclone Thane in southeastern India and identify a complex process of sediment deposition in relation to varied overland flow, and subaerial and subaqueous sediment deposition.

2. Study site

The December 2011 Cyclone Thane struck the southeastern coast of India as a Category 3 cyclone with sustained wind speeds of 140 km/h. The cyclone formed in the central Indian Ocean on 25th December 2011 and intensified as it traversed towards the Indian coastline. Cyclone Thane made landfall between 0630 and 0730 on the 30th December 2011 and caused US$330 million in damages and 47 deaths (CWD, 2012). Cyclone Thane also mobilised vast volumes of sediment from the coastal and nearshore zones and deposited it onshore, typically as washover fans.

The largest subaerially exposed fan (ca. 41,500 m^2) was deposited on Greenery Beach at Thazhamkuda (11°46′16″N, 79°47′36″E), approximately 3 km north of Cuddalore and approximately 20 km south of Puducherry in central Tamil Nadu (Fig. 1a). At the time of fan deposition, Greenery Beach extended north and had completely blocked the northern seaward flowing tributary of the Thenpennai River (also called Ponnaiyar River). The Thenpennai River is an ephemeral river, being dry throughout most of the year except during the monsoon (Mahadev et al., 2022; Mahadev et al., 2019). At this site, the fan breached the low dune and deposited significant volumes of sediment into the slack water. The fan, unfortunately, no longer exists as the Thenpennai River was subsequently reopened in early 2022 (not shown) and the fan has been completely eroded.

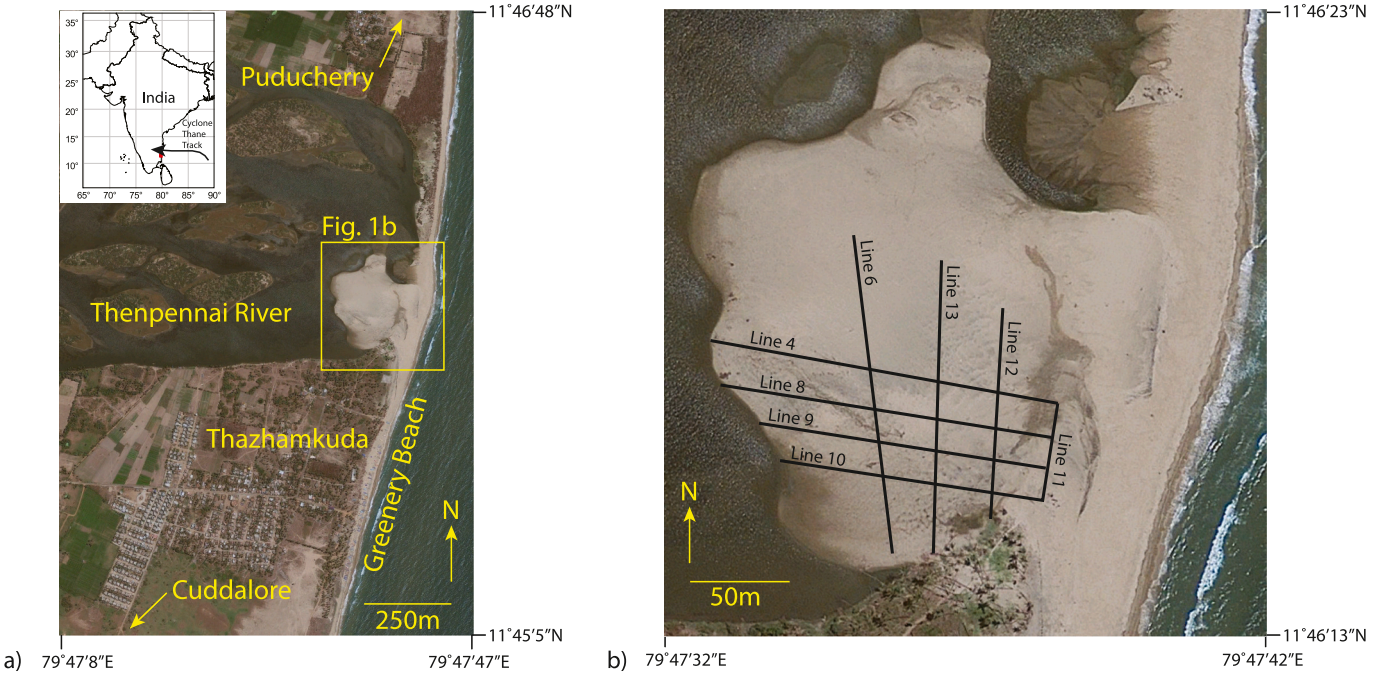

Fig. 1. a) Map of India showing the location of the study site (red box) and the Cyclone Thane track and enlarged region of Thazhamkuda and surrounds, b) detailed satellite image of the Thazhamkuda fan showing the location of the GPR lines. (For interpretation of the references to colour in this figure legend, the reader is referred to the web version of this article.)

3. Methods

3.1. Ground Penetrating Radar profiles

High-frequency GPR (e.g. Gouramanis et al., 2015; Gouramanis et al., 2014), such as 500 or 1000 MHz, images the subsurface stratigraphy at very high spatial and depth resolutions. We collected eight GPR transects on the 24 May 2013 (Fig. 1b) using a 1000 MHz shielded antenna. Four GPR transects were aligned approximately shore normal (Lines 4, 8, 9 and 10) and four transects were aligned approximately shore parallel (lines 6, 11, 12, 13). The antennas were 15 cm apart, the electromagnetic pulse time window was set to 25 ns and the data stacked 4 times. Electromagnetic pulses were emitted and recorded at 1 cm intervals. Only the central portion of the fan was appropriate for GPR examination as this zone formed the topographically highest parts of the fan and recorded data (Fig. 1b). Farther north and south, the fan gently dipped into saline water and the GPR signal suffered attenuation. At these distal margins, the sediment was waterlogged with saline water resulting in loss of the GPR signal.

Although no detailed bathymetry exists for the Thenpennai River slack water before the fan was emplaced, we estimate that the depth was approximately 1 m at the landward margin shallowing to the pre-storm barrier. The sand at the surface was dry, but became saturated with saline water with depth. The 1000 MHz antennas are poor at capturing the groundwater level (e.g. Gouramanis et al., 2015) most likely due to the capillary effect of the water table in porous sands. The saline water of both the Thenpennai River and oceanic water east of the washover fan, resulted in attenuation of the electromagnetic pulse and subsequent loss of signal when the saturation state exceeded 50 % of the pore space between sand grains. Here, we adopt a velocity of 0.15 m/ns in clean sand that produces an approximate vertical resolution ($\lambda/4$) of 1.5 cm, however, finer scale structures can be resolved at the higher frequency component of the electromagnetic pulse (Gouramanis et al., 2015). Unfortunately, a Common Mid-Point survey could not be conducted as the connecting cables do not allow the transmitter and receiver antennas to separate sufficiently.

Topography was collected using a Trimble differential Global Positioning System (dGPS) that was ground-truthed from a surveyed height at a local train station. Due to the relatively flat terrain across the fan, dGPS heights were collected at approximately 10 m increments or where significant breaks in slope occurred. The dGPS measurements have a horizontal accuracy of approximately 1.5 cm and a vertical accuracy of 4 cm.

The GPR images were post-processed using the Ekko Project software from Sensors and Software. Each line was processed identically with dewow with a standard window width of 1.33, background subtraction

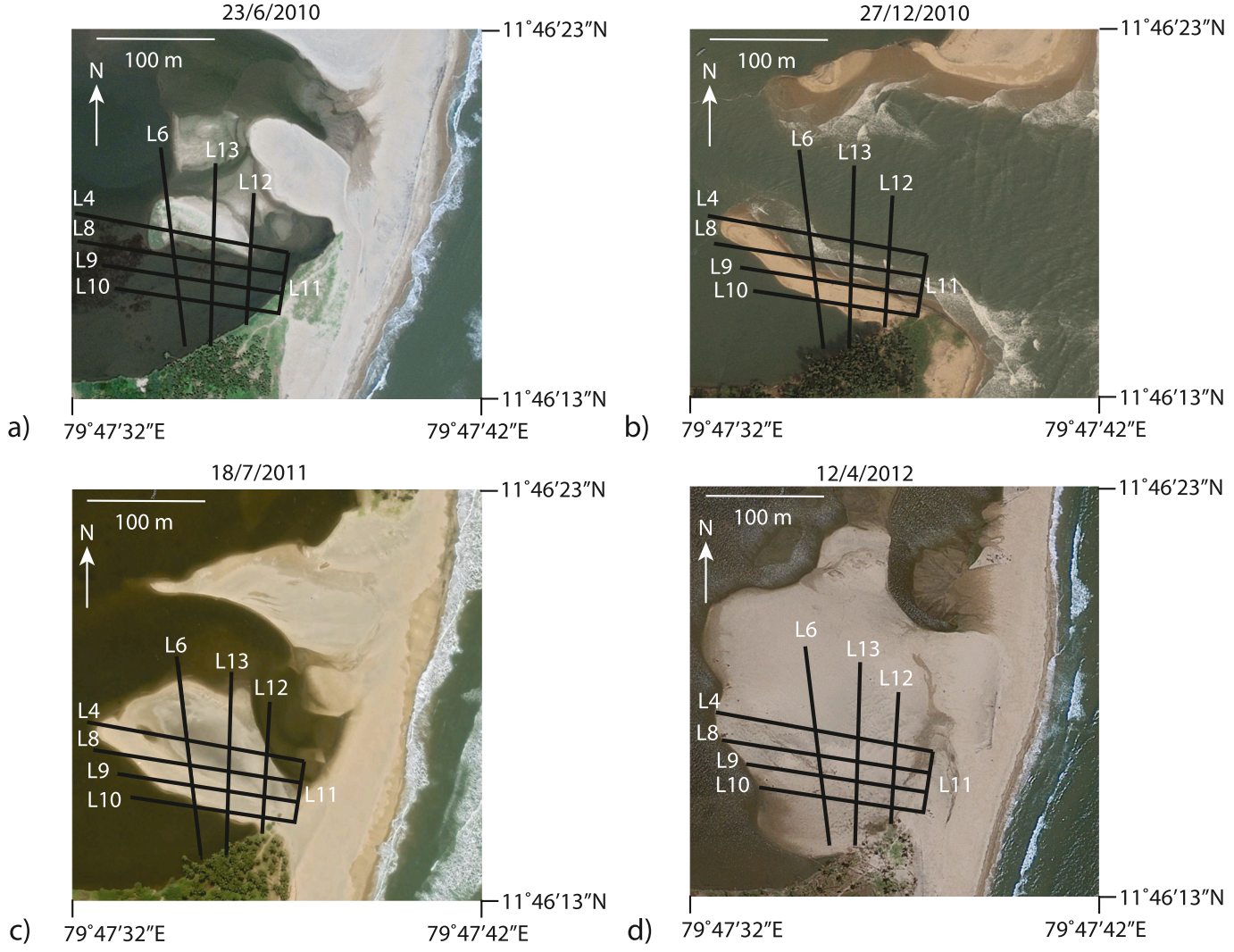

Fig. 2. Satellite imagery of the sequential changes that occurred at the Thenpennai River mouth from a) initially being blocked on 23/6/2010, b) open by 27/12/2010, c) subsequently blocked by 18/7/2011, and d) preserving the 30th December Cyclone Thane washover fan on 12/4/2012.

assuming a rectangular window with a 5 m filter width, automatic gain control with a maximum gain of 2000 with a window width of 1.5 applied, and finally topographically corrected using a velocity of 0.15 m/ns. Background subtraction removed the prominent air and groundwaves, and much of the ringing observed in the pre-processed data. Ringing is now only observed lower down in the profiles where the electromagnetic signal is attenuated, and stratigraphic information not sampled. The removal of the prominent air and groundwaves means the upper 5 to 10 cm of the stratigraphy is uninterpretable noise. GPR profiles are presented with elevation (metres above mean sea level; m amsl) on the left axis, time (ns) on the right axis and distance from the start position along the horizontal axis.

4. Results

4.1. Historical changes

The GoogleEarth satellite images of the fan clearly show that by the 27th December 2010 the Thenpennai River eroded remnants of a previous washover fan and breached the beach barrier, possibly due to a flood (Fig. 2a,b). A tidal channel had formed with sand being deposited landward of the opening. By the 18th July 2011, the Thenpennai River mouth had closed and significant sand deposits had accumulated behind the new beach (Fig. 2c). With the passing of Cyclone Thane over the beach on 31st December 2011, a substantial fan formed in the lagoon behind the modern beach (Fig. 2d). It is with this evolutionary context that we interpret the GPR profiles. For a decade after the formation of the fan, it remained relatively stable with vegetation and minor surficial flooding. The Thenpennai River breached the coastal barrier north of the fan, which was possibly caused by minor flooding in September 2021. By April 2024, the Thenpennai River had migrated south completely eroding the fan (not shown in Fig. 2).

4.2. Radar facies

Within the GPR profiles we identify six radar facies (RF; Table 1). Radar facies describe the observed post-processed characteristics of the electromagnetic spectrum as observed in GPR profiles and are considered to reflect buried sedimentary structures (e.g. Jol and Bristow, 2003; Neal, 2004; Switzer et al., 2020). At the bottom of each profile and near the ends of several profiles there is a zone of little or incoherent data from which stratigraphy cannot be inferred.

4.3. Shore-normal profiles

The four shore-normal profiles (Fig. 3a-d; Lines 4, 8, 9, 10) extend from the neck of the fan landward to the outer edge of the fan and high-resolution stratigraphic data of the fan is inferred from the GPR data.

The central portion of the shore-normal profiles consists of RF2 (Table 1) at approximately 75 to 130 m along Line 4 (Fig. 3a), 45 to 145 m along Line 8 (Fig. 3b), 0 to 130 m along Line 9 (Fig. 3c) and 5 to 65 m along Line 10 (Fig. 3d). Onlapping to the east and west of RF2 on Line 4 (Fig. 3a) are two packets of thick, shallowly dipping (<10°) to slightly concave upwards trapezoidal reflection sequences (RF3; Table 1). Three packets of RF3 are observed onlapping the eastern flank of RF2 and one RF3 packet onlapping to the west on Line 8 (Fig. 3b). Two packets of RF3 onlap RF2 to the west from 115 to 135 along Line 9 (Fig. 3c). One packet of RF3 occurs on the eastern 10 m of Line 10 (Fig. 3d). Narrow (<5 m) to wide (ca. 15 m) concave upwards reflections of RF4 (Table 1) periodically truncate parts of RF2, RF3 and RF5 along each of the shore-normal profiles (Fig. 3). RF5 are moderate length sinuous reflectors that dip from 10 to 30° (Table 1) and typically occur at the western extremities of Line 4 (two packets; Fig. 3a), Line 8 (six packets; Fig. 3b) and Line 9 (four packets; Fig. 3c). The change in gradient of the sinuous reflections coincides with the mean water level. Importantly, these packets often exceed a thickness of 1 m. Infilling RF4, and overlying RF2, RF3 and RF5 and occasionally merging with RF5, are horizontal to sub-horizontal, occasionally wavy reflections that laterally or vertically transition into short dipping (20 to 30°) reflections that constitute RF6 (Fig. 3; Table 1). RF6 can be locally up to 50 cm thick where recognised, but merge upwards to the noise of RF1 at the upper 10 to 15 cm of the profiles (Fig. 3; Table 1).

Table 1
Radar Facies (RF) descriptions and image examples.

Radar Facies (RF)	Example	Example location	Description
RF1		95 to 105 m on Line 6, depth 0 to 0.1 m amsl	RF1 occurs at the top of most profiles where the air and groundwave have been subtracted. Due to the strength of the air and groundwaves, little coherent data is present in the upper ca. 10 cm.
RF2		50 to 140 m on Line 8, depth 0.5 to −0.5 m amsl.	RF2 are long continuous reflections that are concave downwards, often dipping more steeply on one side than the other. To the south of the topographical high in Line 6, these reflections are subparallel to the topography (45 to 57 m on Line 6, depth 0.6 to 0 m amsl).
RF3	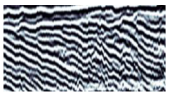	22 to 27 m on Line 11, depth 0.4 to 0 m amsl	RF3 occurs as either shallowly to moderately dipping (<10°) reflections onlapping other packets of RF2.
RF4		127 to 132 m on Line 9, depth 0.5 to 0 m amsl	RF4 are deep convex up reflectors with truncated dipping reflections within.
RF5	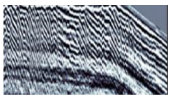	140 to 170 m on Line 8, depth 0.5 to −0.45 m amsl	RF5 are steeply dipping (10 to 30°) reflections that transition to ground surface parallel reflections where ground surface dips towards the slack water at the terminus of the fan.
RF6		6 to 12 m on Line 11, depth 0.4 to 0.1 m amsl	RF6 are a series of short to medium length reflections that are slightly wavy, horizontal to sub-horizontal with short 20 to 30° dipping reflections laterally or above.

4.4. Shore-parallel profiles

The four shore-parallel profiles (Fig. 4a-d; Lines 6, 11, 12, 13) extend from the southern edge of the fan to the north. Profiles 6, 12 and 13 were terminated before the northern edge of the fan as the electromagnetic signal was lost due to salt-water attenuation. Attempts to collect GPR data to the north of these end points failed as the fan topography gently sloped towards the water line and the sediment was saturated just below the fan surface resulting in pooling of saline water as we traversed to the north. Consequently, we were unable to collect data in this region.

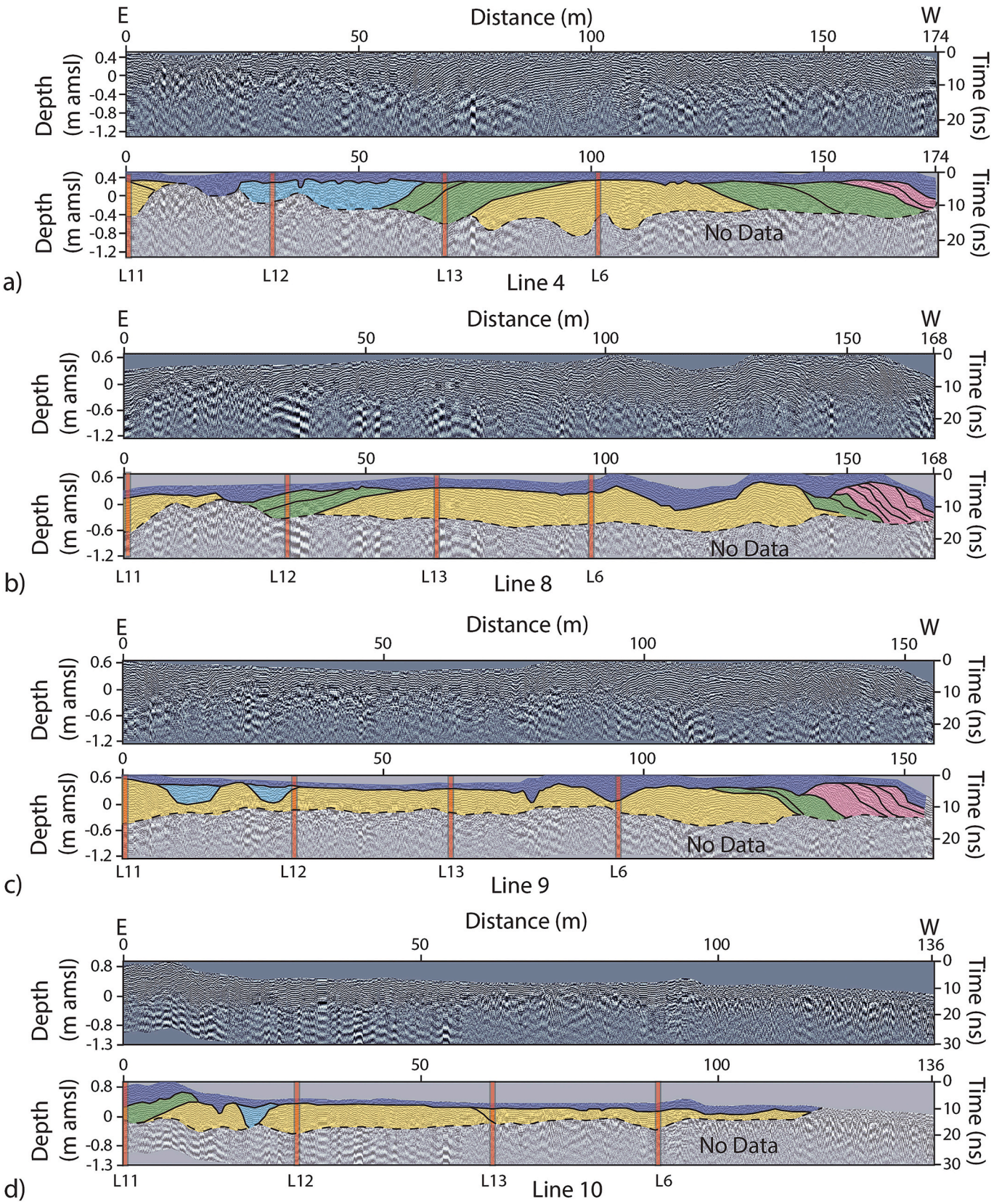

Fig. 3. Shore-normal GPR profiles across the fan presented sequentially from north to south as depicted in Fig. 2; a) Line 4, b) Line 8, c) Line 9, and d) Line 10. Upper panels show processed GPR data and lower panel shows the interpreted radar facies (RF). Red bars depict locations of cross cutting profiles. The colours depicted in the lower panels for all figures represent RFs, with RF1 = No colour as it is too thin (<10 cm) at the air-ground interface, RF2 = Yellow, RF3 = Green, RF4 = Pale Blue, RF5 = Pink, and RF6 = Purple. Solid black lines show distinct contacts within or between RFS, whereas dashed black lines likely show basal contacts at the limits of GPR detection. (For interpretation of the references to colour in this figure legend, the reader is referred to the web version of this article.)

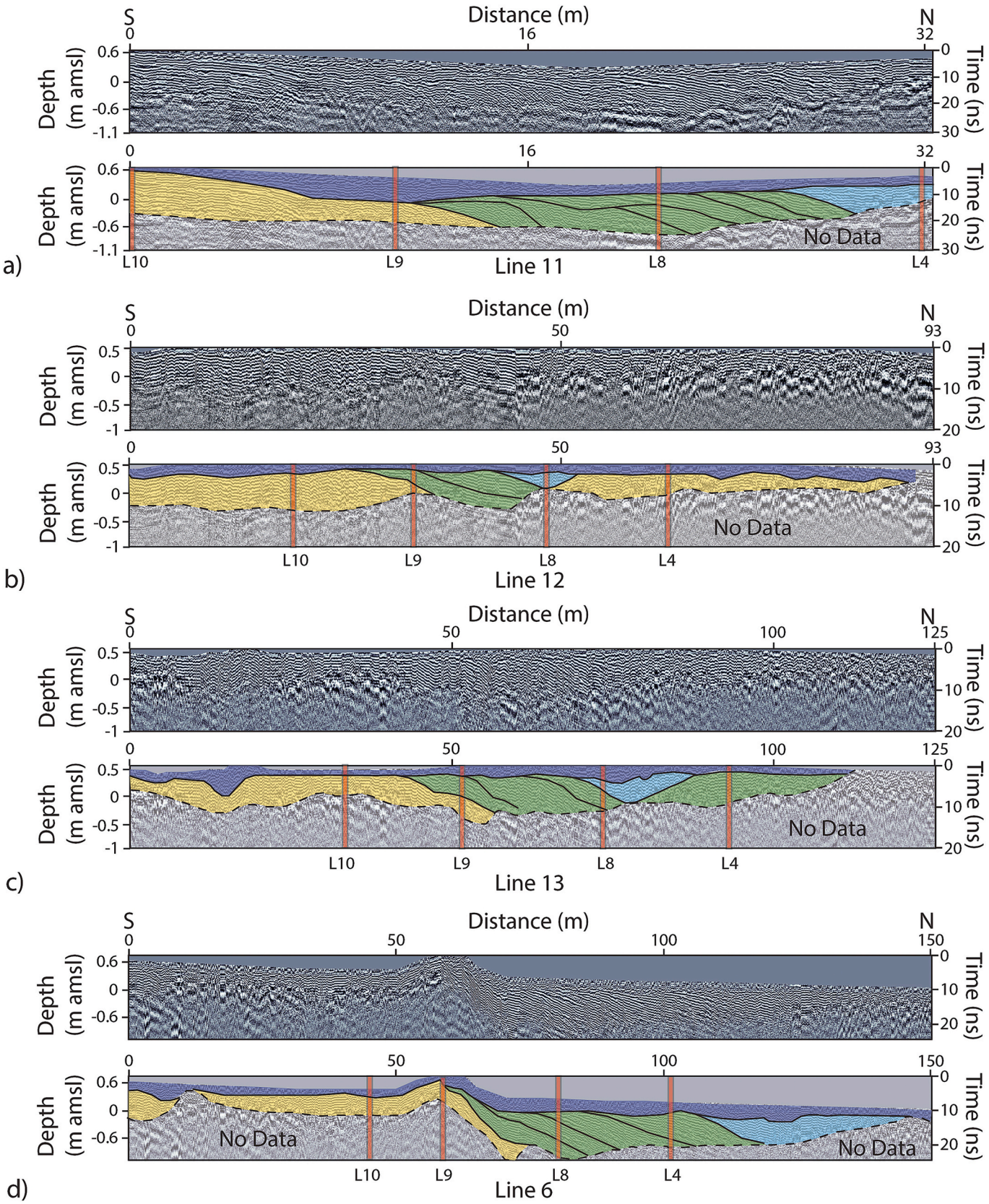

Fig. 4. Shore-parallel GPR profiles across the fan presented sequentially from east to west as depicted in Fig. 2; a) Line 11, b) Line 12, c) Line 13, and d) Line 6. Upper panels show processed GPR data and lower panel shows the interpreted radar facies (RF). Red bars depict locations of cross cutting profiles. Colours and lines as per Fig. 3. (For interpretation of the references to colour in this figure legend, the reader is referred to the web version of this article.)

Where saline water was not near the fan surface, we were able to collect and infer stratigraphic data in high resolution.

The southern sections of the four shore-parallel profiles consist of RF2 (Fig. 4; Table 1). RF2 in Line 11 extends to about 15 m and consists of concave reflections that dip shallowly to the north (Fig. 4a). In lines 12, 13 and 6, RF2 extends from 0 to 40, 55 and 70 m north (Fig. 4b-d). Along Line 13, RF2 reflections reappear at 75 m and dip towards the south and the RF extends north to where the GPR signal becomes attenuated at 115 m (Fig. 4c). Along Line 6, RF2 dips steeply north along the northern edge of the topographical rise at 60 m (Fig. 4d). As with the shore-normal profiles, RF3 (Table 1) onlaps RF2 with long, northerly, shallowly dipping (<10°) reflectors, with Line 11 having six sequential packets (Fig. 4a), Line 12 having two packets (Fig. 4b), Line 13 having three packets (Fig. 4c) and Line 6 having four packets (Fig. 4d). RF4 (Table 1) are present in Line 13 (Fig. 4c) and Line 6 (Fig. 4d) truncating RF2 and RF3. As with the shore-parallel profiles, RF6 (Table 1) infills RF4 and drapes RF2 and RF3 (Fig. 4). RF5 is absent from each of the shore-parallel GPR profiles. RF6 is more challenging to identify in the shore-parallel profiles as it is typically thinner and transitions to RF1 (Table 1) at the top of the GPR profiles. Along Line 11, RF6 is 40 to 50 cm thick between 8 and 12 m, but thins at the extremities (Fig. 4a). RF6 is thin across Lines 12 and 13 (Fig. 4b,c) becoming thicker where it infills small channels. Along Line 6, RF6 is absent or very thin south of the topographic high and thickens to the north of the topographic high (Fig. 4d).

5. Discussion

5.1. Radar facies and depositional interpretation

RF1 occurs across all transects and extends to a depth of 10 cm and represents the removal of the air and groundwaves following background subtraction and is characterised by noise. The strength of the air and groundwaves upon removal resulted in a lack of signal, making stratigraphic interpretation impossible.

RF2 forms a topographic rise in the western half of the fan (Fig. 2). The rise forms the southern subaerially exposed flood tidal channel bank (Fig. 2b). The bank formed following the breaching of the pre-existing sandy barrier by the Thenpennai River, likely due to an increase in either discharge from upstream dams or higher rainfall. Similar features have been observed in aeolian dunes where a small pre-existing structure such as a precursor dune existed (Bristow and Pucillo, 2006; Gouramanis et al., 2020; Clemmensen et al., 2007; Neal and Roberts, 2000; Bristow et al., 2000; Wang and Horwitz, 2006).

RF3 onlaps RF2 in a northerly direction in all profiles (Fig. 4), a westerly direction in lines 4, 8 and 9 (Fig. 3a-c) and an easterly direction in lines 4, 8 and 10 (Fig. 3a,b,d). RF3 formed in two related ways. The first occurred as the northerly dipping sequence (Line 11, Fig. 4a) as Greenery Beach encroached across the Thenpennai River mouth to form the barrier. The second formed as aeolian sediment was deposited on the eastern and western faces of the exposed faces of the flood tidal channel bank after the beach barrier formed. A similar process likely occurred on the southern margin of the northern flood tidal channel bank as is evidenced by the southerly dipping to horizontal reflectors observed in the northern parts of lines 13 and 6 (Fig. 4c,d). In both instances, sediment is deposited both subaqueously and subaerially, infilling the former channel and coalescing to form a pedestal behind Greenery Beach. Much of the sediment required to construct these onlapping facies would likely have originated from the waning flow of the sediment-laden Thenpennai River (Mahadev et al., 2019). Similar radar facies have been observed and the interpretation similar to here in braided bars (e.g. Skelly et al., 2003) and crevasse splays (e.g. Bristow et al., 1999).

RF4 are interpreted as large or small infilled channels. It is unclear whether some of these channels formed before Cyclone Thane either through previous precipitation events or from pre-overwash rainfall from Cyclone Thane. Some channels cut into RF5 and may have formed after the Cyclone Thane overwash as either runout channels or from later rainfall events. Similar radar facies have been identified in numerous coastal environments and interpreted as buried channel structures (e.g. Buynevich et al., 2009; Gouramanis et al., 2020; Okazaki et al., 2015).

RF5 are steeply dipping sigmoidal foresets that transition to parallel to the ground surface at the terminus of the fan. These foresets form as the storm overwash interacts with slack water environments at the landward edge of the fan (Schwartz, 1975; Schwartz, 1982; Morton, 1978; Morton, 1979). The terminal foresets can be formed either entirely subaerially (May et al., 2017; Morton, 1978; Morton, 1979; Wang and Horwitz, 2006; Schwartz, 1975), entirely subaqueously (Schwartz, 1975) or both subaerially and subaqueously (Wang and Horwitz, 2006). They can range in height from <0.3 m (Schwartz, 1975) to over 2 m (Wang and Horwitz, 2006). At Thazhamkuda, the terminal foresets are steepest at the water level and become shallower in deeper water giving them a distinct sigmoidal shape. Other GPR studies of storm fans have not recognised this radar facies (e.g. Soria et al., 2021; Switzer and Jones, 2008).

Terminal foresets (RF5) have not been recognised in tsunami sedimentary deposits to date. Until they are identified from recent tsunami deposits, we propose that terminal foresets, when present, are diagnostic sedimentary structures to distinguish storm from tsunami deposited sediments. Unfortunately, this facies is not ubiquitous in storm deposits, but when observed and correctly interpreted, can be diagnostic. The location of terminal foresets in a fan provides direct evidence of the maximum extent of the storm fan deposition and evidence that the fan was deposited in a subaqueous environment at its distal margins (e.g. Schwartz, 1975; Schwartz, 1982).

RF6 represent planar laminated sands and tabular or trough cross beds at the top of the fan sequence. These reflect tabular cross beds that have migrated across the dune as the overwash waned. Schwartz (1982) observed linguoid ripples along the surface of storm fans and inferred these to be formed by low-flow regime parallel to the predominant overwash direction. Switzer et al. (2012) identified similar structures in their analysis of the 2004 Indian Ocean Tsunami deposit from Silver Beach located approximately 3.5 km south of Thazhamkuda. Switzer et al. (2012) interpreted the sediments as formed by the tsunami waters forming small channels as it drained from the tsunami sandsheet. RF6 is not fully captured as the upper part is not recorded due to the noise produced by the removal of the air and groundwaves (RF1).

The formation of the pedestal and Cyclone Thane fan are captured in the conceptual model in Fig. 5.

5.2. Washover fan deposition

The washover fan we examined using GPR from the southeastern coast of India is the first fan to be examined using high frequency GPR. Broadly speaking the GPR analysis shows some strong similarities with the canonical storm fans described from the southern United States of America (e.g. Schwartz, 1975; Schwartz, 1982; Morton, 1978; Morton, 1979; Sedgwick and Davis, 2003). These similarities include buried infilled channels (RF4), planar, tabular and trough cross beds (RF5) and terminal foresets (RF6).

The recognition of the topographic highs interpreted as flood tidal channel bank deposits (RF2) funnelled the deposition of sediment into the blocked tidal channel prior to Cyclone Thane. These onlapping surfaces (RF3) coalesced as sand pulses were trapped behind the barrier. This built a subaerially exposed pedestal for the Cyclone Thane overwash to deposit sediment on and to extend the pedestal westwards with the deposition of terminal foresets (RF5). Upon the pedestal, the fan sediments show a combination of short linear structures inferred to be horizontal bedding or planar laminations transitioning to trough and tabular cross-beds laterally and vertically (RF6).

Whereas the canonical fan model (Schwartz, 1975; Schwartz, 1982; Sedgwick and Davis, 2003) implies significant horizontal or very

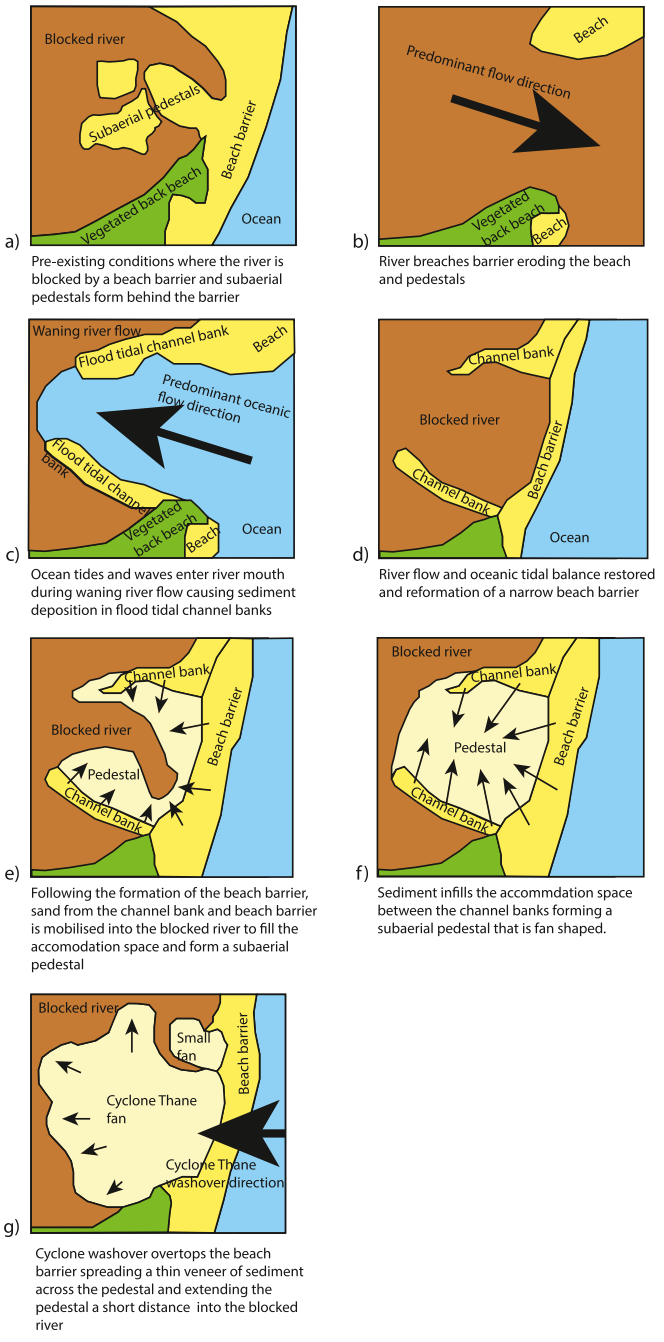

Fig. 5. Conceptual model for the formation the pedestal following erosion and reformation of the Thazhamkuda beach barrier and the subsequent overtopping and deposition of the fan sediments on and around the pedestal. Large arrows show predominant tidal and wave directions and the direction from which Cyclone Thane approached the coast. Small arrows signify predominant directions of sediment movement.

shallow, landward-dipping laminations, the horizontal reflections inferred to be laminations are comparatively short and typically occur where there was a topographic depression in the pedestal surface. Wang and Horwitz (2006) and May et al. (2017) identify extensive horizontal and subhorizontal reflections in their examination of storm fans, but these fans were predominantly deposited subaerially. From our analysis, we postulate that horizontal laminations in storm fans are restricted to only those parts of the fan that are deposited entirely subaerially.

Upon initial inspection, the fan at Thazhamkuda appeared to be the largest fan (ca. 41,500 m^2) deposited by Cyclone Thane along the Tamil Nadu coastline. However, after our GPR assessment, the presence of the pre-Cyclone Thane pedestal significantly controlled the style and location of sediment deposition. Although Cyclone Thane was a significant event, it only contributed approximately 20 m to the growth of the pedestal and < 0.5 m to the overall vertical height of the pedestal. This implies that although the Tamil Nadu coastline is a sediment-rich environment, Cyclone Thane did not mobilise and redeposit large volumes of sediment at this site unlike other major storms (e.g. Hayes, 1967; May et al., 2017; Schwartz, 1975; Sedgwick and Davis, 2003; Wang and Horwitz, 2006). It is thus prudent for coastal hazard specialists to have a deep appreciation of the pre-existing conditions when evaluating the impacts of coastal hazards as pre-existing conditions strongly influence the degree and patterns of sedimentation.

6. Conclusion

Storm deposits that form fans are major contributors to the redistribution of both offshore and onshore coastal sediments. Storm fans have been characterised from numerous coastlines around the world and the mode of deposition have been characterised from onshore records. The fan we examined at Thazhamkuda, near Cuddalore on the coast of southeast India was deposited partially subaerially on beach barrier that blocked the Thenpennai River, and partially within the Thenpennai River. Of note, this fan was the largest fan to be deposited along the Tamil Nadu coastline (ca. 41,500 m^2) during the 31st December 2011 Cyclone Thane, and thus, a prime location to examine storm deposits using very high frequency (1000 MHz) GPR and satellite imagery.

However, the size of the fan was misleading as the site was primed for the deposition of the Cyclone Thane washover fan through the formation of a subaerial pedestal behind the blocked Thenpennai River. Prior to Cyclone Thane, the Thenpennai River breached the former Greenery Beach forming a large flood tidal channel. Following the breaching event, flow in the Thenpennai River subsided and a sand body rapidly reformed the Greenery Beach barrier. With the development of low energy conditions, the northern and southern flood tidal channel banks and the beach barrier that connected them served as nucleation points for a rapid infilling and formation of a subaerial pedestal. This pedestal formed the platform upon which Cyclone Thane overwash deposited sediment on top and at the distal margins of the pedestal.

The Cyclone Thane washover event deposited a < 30 cm deposit across the pedestal consisting of moderate lengths of horizontal beds and planar laminations that transition horizontally and vertically to tabular and trough cross beds. Cyclonic rainfall eroded shallow channels across the fan, both prior to the overwash event and in the aftermath of the overwash forming runout facies. At the landward terminus of the fan where the fan is in contact with the Thenpennai River slackwater, very thick (up to 1 m high) terminal foresets are recorded. Importantly, the terminal foresets only extend the margins of the fan by up to 20 m. Although not found along all of the margins of the Thazhamkuda fan, and not ubiquitous to storm washover fans, terminal foresets remain one of the few discriminating features between storm and tsunami deposits as this structure has yet to be identified in known tsunami deposits. The careful analysis of washover deposits along susceptible coastlines, commonly involves attempting to discriminate between storm and tsunami deposits in the geological record. If successful such information can be used identify the frequency and the type of overwash that is known to occur and this knowledge will greatly improve priorities and practices for managing coastal systems, communities and infrastructure.

CRediT authorship contribution statement

Chris Gouramanis: Writing – original draft, Visualization, Project administration, Methodology, Investigation, Funding acquisition, Formal analysis, Data curation, Conceptualization. **Seshachalam Srinivasalu:** Writing – review & editing, Project administration,

Methodology, Investigation. **Andasabari Karthik:** Writing – review & editing, Project administration, Methodology, Investigation. **Dat T. Pham:** Writing – original draft, Methodology, Investigation. **Stephen Carson:** Writing – review & editing, Methodology, Investigation. **Adam D. Switzer:** Writing – review & editing, Funding acquisition, Conceptualization.

Declaration of competing interest

The authors declare that they have no known competing financial interests or personal relationships that could have appeared to influence the work reported in this paper.

Acknowledgements

CG, PTD, and ADS thank the staff of Anna University for hosting them during fieldwork. This research was supported by funding from Singapore Ministry of Education (Grant No: R-109-000-248-115) awarded to C.G. and Singapore National Research Foundation fellowship scheme (Grant No: NRF-RF2010-04) awarded to A.D.S. The authors wish to thank Prof. Shu Gao for editorial handling and to thank two anonymous reviewers for their constructive feedback on an earlier version of this manuscript.

Data availability

The raw GPR and topography data are available from the ANU Data Commons at DOI:10.25911/vc3s-xy72.

References

Benamri, S., Costa, P.J.M., Zaghloul, M.N., Mercier, J.L., Abbassi, A., El Mourabet, M., Aboumaria, K., 2023. Provenance and sedimentary processes on Pleistocene storm deposits in Harhoura (Northern Coastal Atlantic, Morocco): new constraints from a source to sink perspective. Mar. Geol. 457.

Brill, D., May, S.M., Engel, M., Reyes, M., Pint, A., Opitz, S., Dierick, M., Gonzalo, L.A., Esser, S., BRÜCKNER, H., 2016. Typhoon Haiyan's sedimentary record in coastal environments of the Philippines and its palaeotempestological implications. Nat. Hazards Earth Syst. Sci. 16, 2799–2822.

Bristow, C.S., 2013. 14.16 Ground Penetrating Radar. Treatise on Geomorphology.

Bristow, C.S., Pucillo, K., 2006. Quantifying rates of coastal progradation from sediment volume using GPR and OSL: the Holocene fill of Guichen Bay, south-east South Australia. Sedimentology 53, 769–788.

Bristow, C.S., Skelly, R.L., Ethridge, F.G., 1999. Crevasse splays from the rapidly aggrading, sand-bed, braided Niobrara River, Nebraska Effect of base-level rise. Sedimentology 46, 1029–1047.

Bristow, C.S., Bailey, S.D., Lancaster, N., 2000. The sedimentary structures of linear sand dunes. Nature 406, 56–59.

Buynevich, I., Jol, H.M., Fitzgerald, D.M., 2009. Coastal environments. In: Jol, H.M. (Ed.), Ground Penetrating Radar Theory and Applications.

Buynevich, I.V., Fitzgerald, D.M., Goble, R.J., 2007. A 1500 yr record of North Atlantic storm activity based on optically dated relict beach scarps. Geology 35.

Clemmensen, L.B., Bjørnsen, M., Murray, A., Pedersen, K., 2007. Formation of aeolian dunes on Anholt, Denmark since AD 1560: a record of deforestation and increased storminess. Sediment. Geol. 199, 171–187.

CWD, 2012. Very Severe Cyclonic Storm THANE over the Bay of Bengal - A Report. Cyclone Warning Division, Ministry of Earth Sciences, Government of India, India.

Dixon, S., Green, A., Cooper, A., 2015. Storm Swash deposition on an embayed rock coastline: facies, formative mechanisms, and preservation. J. Sediment. Res. 85, 1155–1165.

Donnelly, J.P., Woodruff, J.D., 2007. Intense hurricane activity over the past 5,000 years controlled by El Nino and the West African monsoon. Nature 447, 465–468.

Donnelly, J.P., Bryant, S.S., Butler, J., Dowling, J., Fan, L., Hausmann, N., Newby, P., Shuman, B., Stern, J., Westover, K., Webb III, T., 2001. 700 yr sedimentary record of intense hurrican landfalls in southern New England. Geol. Soc. Am. Bull. 113, 714–727.

Ganzei, L.A., Razzhigaeva, N.G., Harlamov, A.A., Ivel'skaya, T.N., 2010. Extreme storms in 2006–2007 on Shikotan Island and their impact on the coastal relief and deposits. Oceanology 50, 425–434.

Gouramanis, C., Switzer, A.D., Pham, D.T., Bristow, C.S., Jankaew, K., Rubin, C.M., Lee, Y.S., 2014. Thin-bed Ground-Penetrating Radar analysis of preserved modern and palaeotsunami deposits from Phra Thong Island, Thailand. In: Proceedings of the 15th International Conference on Ground Penetrating Radar, pp. 1047–1052.

Gouramanis, C., Switzer, A.D., Polivka, P.M., Bristow, C.S., Jankaew, K., Dat, P.T., Pile, J., Rubin, C.M., Yingsin, L., Ildefonso, S.R., Jol, H.M., 2015. Ground penetrating radar examination of thin tsunami beds — A case study from Phra Thong Island, Thailand. Sediment. Geol. 329, 149–165.

Gouramanis, C., Switzer, A.D., Jankaew, K., Bristow, C.S., Pham, D.T., Ildefonso, S.R., 2017. High-frequency coastal overwash deposits from phra Thong Island, Thailand. Sci. Rep. 7, 43742.

Gouramanis, C., Switzer, A.D., Bristow, C.S., Pham, D.T., Mauz, B., Hoang, Q.D., Lam, D. D., Lee, Y.S., Soria, J.L.A., Pile, J., Chi, N.T.K., Nghiem, D., Sloss, C., 2020. Holocene evolution of the Chan May coastal embayment, central Vietnam: Changing coastal dynamics associated with decreasing rates of progradation possibly forced by mid- to late-Holocene sea-level changes. Geomorphology 367.

Gouramanis, C., Karthik, A., Srinivasalu, S., Carson, S., Switzer, A.D., 2024. Bayesian statistical analysis reveals spatial heterogeneity in Cyclone Thane deposits from Southeast India. Mar. Geol. 478.

Haque, M.M., Yamada, M., Uchiyama, S., Hoyanagi, K., 2021. Depositional setup and characteristics of the storm deposit by the 2007 Cyclone Sidr on Kuakata Coast, Bangladesh. Mar. Geol. 442.

Hayes, M.O., 1967. Hurricanes as geological agents Case studies of Hurricanes Carla 1961 and Cindy 1963. In: Report on Investigations. Bureau of Economic Geology, University of Texas, Texas, USA.

Hong, I., Pilarczyk, J.E., Horton, B.P., Fritz, H.M., Kosciuch, T.J., Wallace, D.J., Dike, C., Rarai, A., Harrison, M.J., Jockley, F.R., 2018. Sedimentological characteristics of the 2015 Tropical Cyclone Pam overwash sediments from Vanuatu, South Pacific. Mar. Geol. 396, 205–214.

Jol, H.M., Bristow, C.S., 2003. GPR in sediments: advice on data collection, basic processing and interpretation, a good practice guide. Geol. Soc. Lond., Spec. Publ. 211, 9–27.

Kortekaas, S., Dawson, A.G., 2007. Distinguishing tsunami and storm deposits: an example from Martinhal, SW Portugal. Sediment. Geol. 200, 208–221.

Kosciuch, T.J., Pilarczyk, J.E., Hong, I., Fritz, H.M., Horton, B.P., Rarai, A., Harrison, M. J., Jockley, F.R., 2018. Foraminifera reveal a shallow nearshore origin for overwash sediments deposited by Tropical Cyclone Pam in Vanuatu (South Pacific). Mar. Geol. 396, 171–185.

Leatherman, S.P., Williams, A.T., 1977. Lateral textural grading in washover sediments. Earth Surface Proc. 2, 333–341.

Leatherman, S.P., Williams, A.T., Fisher, J.S., 1977. Overwash sedimentation associated with a large-scale northeaster. Mar. Geol. 24, 109–121.

Lindhorst, S., Betzler, C., Hass, H.C., 2008. The sedimentary architecture of a Holocene barrier spit (Sylt, German Bight): Swash-bar accretion and storm erosion. Sediment. Geol. 206, 1–16.

Liu, K.-B., Fearn, M.L., 1993. Lake-sediment record of late Holocene hurricane activities from coastal Alabama. Geology 21, 793–796.

Liu, K.-B., Fearn, M.L., 2000. Reconstruction of prehistoric landfall frequencies of catastrophic hurricanes in Northwestern Florida from Lake Sediment Records. Quat. Res. 54, 238–245.

Mahadev, Singh, A.K., Jaiswal, M.K., 2019. Application of luminescence age models to heterogeneously bleached quartz grains from flood deposits in Tamilnadu, southern India: reconstruction of past flooding. Quat. Int. 513, 95–106.

Mahadev, Jaiswal, M.K., Shivsager, V., Singh, S., Singh, A.K., 2022. Late quaternary evolution of lower Kaveri and adjoining river basins in Tamil Nadu, Southern India: a combined approach using remote sensing and optical dating of fluvial records. Environ. Chall. 9.

May, S.M., Brill, D., Leopold, M., Callow, J.N., Engel, M., Scheffers, A., Opitz, S., Norpoth, M., Brückner, H., 2017. Chronostratigraphy and geomorphology of washover fans in the Exmouth Gulf (NW Australia) – A record of tropical cyclone activity during the late Holocene. Quat. Sci. Rev. 169, 65–84.

Morton, R.A., 1978. Large-scale rhomboid bed forms and sedimentary structures associated with hurricane washover. Sedimentology 25, 183–204.

Morton, R.A., 1979. Subaerial storm deposits formed on barrier flats by wind-driven currents. Sediment. Geol. 24, 105–122.

Morton, R.A., Sallenger, A.H., 2003. Morphological impacts of extreme storms on sandy beaches and barriers. J. Coast. Res. 19, 560–573.

Morton, R.A., Gelfenbaum, G., Jaffe, B.E., 2007. Physical criteria for distinguishing sandy tsunami and storm deposits using modern examples. Sediment. Geol. 200, 184–207.

Neal, A., 2004. Ground-penetrating radar and its use in sedimentology: principles, problems and progress. Earth Sci. Rev. 66, 261–330.

Neal, A., Roberts, C.L., 2000. Applications of ground-penetrating radar (GPR) to sedimentological, geomorphological and geoarchaeological studies in coastal environments. Geol. Soc. Lond., Spec. Publ. 175, 139–171.

Okazaki, H., Kwak, Y., Tamura, T., 2015. Depositional and erosional architectures of gravelly braid bar formed by a flood in the Abe River, central Japan, inferred from a three-dimensional ground-penetrating radar analysis. Sediment. Geol. 324, 32–46.

Pattiaratchi, C.B., Wijeratne, E.M., 2015. Are meteotsunamis an underrated hazard? Philos. Trans. A Math Phys. Eng. Sci. 373.

Pham, D.T., Gouramanis, C., Switzer, A.D., Rubin, C.M., Jones, B.G., Jankaew, K., Carr, P.F., 2017. Elemental and mineralogical analysis of marine and coastal sediments from Phra Thong Island, Thailand: Insights into the provenance of coastal hazard deposits. Mar. Geol. 385, 274–292.

Phantuwongraj, S., Choowong, M., 2011. Tsunamis versus storm deposits from Thailand. Nat. Hazards 63, 31–50.

Phantuwongraj, S., Choowong, M., Nanayama, F., Hisada, K.-I., Charusiri, P., Chutakositkanon, V., Pailoplee, S., Chabangbon, A., 2013. Coastal geomorphic conditions and styles of storm surge washover deposits from Southern Thailand. Geomorphology 192, 43–58.

Rodriguez, A.B., Theuerkauf, E.J., Ridge, J.T., Vandusen, B.M., Fegley, S.R., 2020. Long-term washover fan accretion on a transgressive barrier island challenges the assumption that paleotempestites represent individual tropical cyclones. Sci. Rep. 10, 19755.

Schwartz, R.K., 1975. Nature and Genesis of Some Washover Deposits. Department of the Army, U.S.
Schwartz, R.K., 1982. Bedform and strati¢cation characteristics of some modern small-scale washover sand deposits. Sedimentology 29, 835–849.
Sedgwick, P.E., Davis, R.A., 2003. Stratigraphy of washover deposits in Florida: implications for recognition in the stratigraphic record. Mar. Geol. 200, 31–48.
Skelly, R.L., Bristow, C.S., Ethridge, F.G., 2003. Architecture of channel-belt deposits in an aggrading shallow sandbed braided river: the lower Niobrara River, northeast Nebraska. Sediment. Geol. 158, 249–270.
Soria, J.L.A., Switzer, A.D., Villanoy, C.L., Fritz, H.M., Bilgera, P.H.T., Cabrera, O.C., Siringan, F.P., Maria, Y.Y.-S., Ramos, R.D., Fernandez, I.Q., 2016. Repeat storm surge disasters of Typhoon Haiyan and Its 1897 Predecessor in the Philippines. Bull. Am. Meteorol. Soc. 97, 31–48.
Soria, J.L.A., Switzer, A.D., Pilarczyk, J.E., Siringan, F.P., Khan, N.S., Fritz, H.M., 2017. Typhoon Haiyan overwash sediments from Leyte Gulf coastlines show local spatial variations with hybrid storm and tsunami signatures. Sediment. Geol. 358, 121–138.
Soria, J.L.A., Switzer, A.D., Pile, J., Siringan, F.P., Brill, D., Daag, A., 2021. Geomorphological and sedimentological records of recent storms on a volcaniclastic coast in Bicol, Philippines. Geomorphology 386.
Switzer, A.D., Jones, B.G., 2008. Setup, deposition, and sedimentary characteristics of two storm overwash deposits, Abrahams Bosom Beach, Southeastern Australia. J. Coast. Res. 1, 189–200.
Switzer, A.D., Srinivasalu, S., Thangadurai, N., Ram Mohan, V., 2012. Bedding structures in Indian tsunami deposits that provide clues to the dynamics of tsunami inundation. Geol. Soc. Lond., Spec. Publ. 361, 61–77.
Switzer, A.D., Gouramanis, C., Bristow, C.S., Simms, A.R., 2020. Ground-penetrating radar (GPR) in coastal hazard studies. Geological Records of Tsunamis and Other Extreme Waves 143–168. https://doi.org/10.1016/B978-0-12-815686-5.00008-0.
Wang, P., Horwitz, M.H., 2006. Erosional and depositional characteristics of regional overwash deposits caused by multiple hurricanes. Sedimentology 54, 545–564.
Yap, W., Switzer, A.D., Gouramanis, C., Marzinelli, E., Wijaya, W., Yan, Y.T., Dominey-Howes, D., Labbate, M., Srinivasalu, S., Jankaew, K., Lauro, F.M., 2021. Environmental DNA signatures distinguish between tsunami and storm deposition in overwash sand. Commun. Earth Environ. 2.